Loss of solar wind plasma neutrality and affect on surface potentials near the lunar terminator and shadowed polar regions

W. M. Farrell,[1] T. J. Stubbs,[1,2] J. S. Halekas,[3] G. T. Delory,[3] M. R. Collier,[1] R. R. Vondrak,[1] and R. P. Lin[3]

Received 14 November 2007; revised 7 January 2008; accepted 21 January 2008; published 13 March 2008.

[1] As the solar wind is absorbed on the lunar dayside, a clear and obvious plasma void is created in the anti-solar direction that extends many lunar radii behind the Moon. Plasma adjacent to this void will expand into the depleted region and this process is modeled here using a particle-in-cell code. It is found that thermal electrons will diffuse into the void ahead of the ions, creating a break in plasma quasi-neutrality. In essence, immediately trailing behind the lunar terminator/polar regions, there is a magnetic-field aligned E-field peaking near 400 mV/m associated with a standing double-layer, this layer consisting of fast thermal electrons (electron cloud) moving into the central void ahead of an ion-enhanced layer. We demonstrate that the surface locations that are incident with the electron cloud (just nightside of the terminator) will develop enhanced negative surface potentials due to the dominance of electron currents. Such regions of large negative potentials near the lunar poles are of interest, especially given NASA's recent announcement of a lunar outpost at the south polar Aitken Basin. **Citation:** Farrell, W. M., T. J. Stubbs, J. S. Halekas, G. T. Delory, M. R. Collier, R. R. Vondrak, and R. P. Lin (2008), Loss of solar wind plasma neutrality and affect on surface potentials near the lunar terminator and shadowed polar regions, *Geophys. Res. Lett.*, *35*, L05105, doi:10.1029/2007GL032653.

1. Introduction

[2] Recently, The NASA Constellation Program Lunar Architecture Team (LAT) identified a potential human outpost location at the permanently sun lit edge of Shackleton crater. This site has many advantages including consistent solar power, thermal stability, and a nearby source of possible water (or hydrogen) for resource utilization. However, since the pole resides near the terminator, the site is also a likely location of increased energetic dust activity [*Berg et al.*, 1976] possibly associated with anomalous electrostatic fields that form in the region [*Farrell et al.*, 2007]. We discuss herein a further complication of the near-terminator electrical environment: the loss of local solar wind plasma neutrality in forming the trailing lunar wake.

[3] The lunar terminator region is an electrically-active location. Driven by current balance between photoelectrons and solar wind plasma, there is a substantial surface potential change from dayside-positive to nightside-negative in the region [*Manka*, 1973, *Stubbs et al.*, 2006]. At sub-solar angles approaching 90°, photoelectric currents charge the surface a few volts positive. On the nightside, electron plasma currents charge the surface negative. However, because of lunar wake effects (that vastly reduce the electron density and increase the electron temperature) the nightside terminator surface potentials can become strongly negative, with modeled values below −100 V [*Farrell et al.*, 2007]. The wake forms because the Moon absorbs the supersonic solar wind on the dayside, leaving a trailing void in the anti-sunward directed flow. The Suprthremal Ion Detector Experiment (SIDE) landed package reported measured surface potentials <−100 V near the terminator [*Benson*, 1977]. Lunar Prospector electron observations confirm a consistent solar wind-to-wake potential difference of many hundreds of volts (negative) [*Halekas et al.*, 2005].

[4] Previous analytical modeling of nightside/terminator potentials have applied a self-similar quasi-neutral approximation for wake density [*Samir et al.*, 1983; *Halekas et al.*, 2005; *Farrell et al.*, 2007]. A potential is calculated, but quasi-neutrality $n_e = n_i$ is forced on the solution (plasma quasi-neutrality is defined such that on scale sizes larger than the plasma Debye length the electrons and ion densities are equal). However, self-consistent electrostatic simulations of plasma expansion [*Crow et al.*, 1975; *Farrell et al.*, 1998; *Birch and Chapman*, 2001a, 2001b] that relax the quasi-neutrality constraint indicate that neutrality is severely compromised near the terminator-origin of the wake.

[5] Specifically, immediately downstream from the terminator along the wake flank, solar wind electrons will thermally-diffuse into the wake along the cross-wake magnetic field component ahead of the more-massive ions. An electron cloud thus precedes the inflowing plasma [*Crow et al.*, 1975]. An ambipolar E-field is established that retards electron motion and accelerates ions. Cross-tail ion beams form from these fields and are the keynote feature of the ambipolar process. Such beams have been observed in the wake of the moon [*Ogilvie et al.*, 1996] and the space shuttle [*Singh et al.*, 1989] suggesting both regions replenish their plasma depletions via the same neutrality-destroying process.

[6] The objective of this work is to examine in detail the loss of plasma quasi-neutrality along the wake flanks. Using the particle-in cell code applied previously by *Farrell et al.* [1998] for lunar wake applications we will examine the migration of the ambipolar-created electron cloud into the nightside region. We will especially emphasize the near-Moon regions where the ambipolar non-neutral plasma comes in contact with the lunar surface. We will demon-

[1]Solar System Exploration Division, NASA Goddard Space Flight Center, Greenbelt, Maryland, USA.
[2]Goddard Earth Science and Technology Center, University of Maryland Baltimore County, Baltimore, Maryland, USA.
[3]Space Science Laboratory, University of California, Berkeley, California, USA.

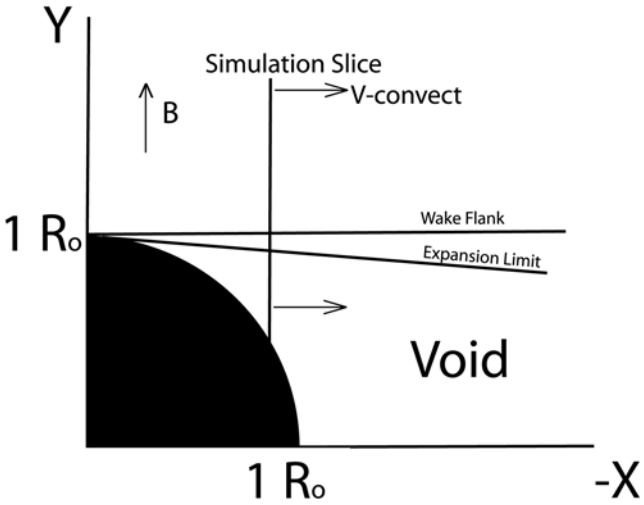

Figure 1. An illustration of the simulation geometry as applied to an obstacle of radius R_o in a flowing plasma.

strate that the lunar surface potentials will change substantially compared to neutral estimates.

2. Simulation Description

[7] A complete description of the particle-in-cell (PIC) code is given by *Farrell et al.* [1998]. The geometry is illustrated in Figure 1. We define the X-axis as that aligned anti-parallel to the flow of the plasma (solar wind) with +X pointing toward the flow source (sun) and the Y as an axis perpendicular to the plasma flow. The code is a 1-D electrostatic simulation along the Y-axis using 20000 ions and electrons in a 500 Debye length space with motion allowed along V_y. This simulation system can be considered a "slice" of plasma aligned along the Y-axis. The magnetic field is also assumed to be aligned along this axis as well, and hence magnetic forces do not directly affect particle dynamics. While this constraint may seem restrictive, the model applies as long as there is some cross-wake B component (B_y), which allows thermal plasma to flow inward to the wake. The simulated ion to electron mass ratio is 20:1.

[8] An initial plasma void is created in the simulation, this of 125 Debye lengths in width (corresponding to an equivalent obstacle diameter, 2 R_o, where R_o is defined here as an obstacle radius). The surface creating the void is not explicitly included in the simulation. Instead, we have the initial condition that a plasma void is present (assumed to be formed by solar wind absorption at the Moon) and we then simulate the subsequent evolution of the plasma dynamics in response to the void.

[9] The property of the solar wind plasma that allows a 2-D rendering of the wake is the solar wind plasma convection past the obstacle that is considered time-stationary in the obstacle (i.e., lunar) frame-of-reference (see Figure 1). In the simulations, we assume the slice of plasma along the Y-axis convects down the wake tail with a convection speed of $V_c = X/t$. Hence, the evolution of the slice in time corresponds to a specific X location down the tail via $X = V_c\, t$. Specifically, at time $t = 0$, the plasma slice is located at $X = 0\ R_o$ and the slice mimics the wake at its source point (i.e., a perfect step function dropout in plasma density). At some later time, the electrostatically-evolved slice is representative of the plasma located at an X value further down the tail. The X/t relationship is $X = -8.75 \times 10^{-2}\ R_o\, t$ (see derivation by *Farrell et al.* [1998]) where t is in units of inverse simulated plasma periods. Stacking the observations of a Y-axis "slice" in time, one can easily convert to X via the X/t relationship, and thus generate the 2-D X-Y renderings of simulation results. Previous applications of this technique produced very close matches to real observations (like those from the Wind spacecraft [see *Farrell et al.*, 1998, Plate 3; *Birch and Chapman*, 2001a, Figure 5]).

[10] While the lunar surface is not included in this simulation, we can still derive surface potentials using simulation results. To explicitly derive lunar-like surface potentials, we perform two steps: First, we identify locations in the simulation where a spherical surface would lie (consistent with the nightside lunar location) and examine the wake plasma at these points. Second, we then perform analytical current balance calculations [see *Manka*, 1973, appendix] to derive the surface charging as if the surface was present, but now using the simulated electron and ion values as inputs representing the near-surface plasma.

3. Results

[11] Figure 2 shows the simulated (a) ion density, (b) electron density, (c) their difference, and (d) associated ambipolar E-field in the downstream wake region. The solar wind is assumed to stream from the left side of the figure. The initial plasma void created by the obstacle (Moon) is located at $X = 0\ R_o$ and we simulate the flow out to 2 R_o behind the obstacle. More distant renderings of this wake (out to >32 R_o) were presented by *Farrell et al.* [1998]. We focus on the region near the obstacle, where the ambipolar field is most intense.

[12] The electron cloud migrating into the wake (ahead of the ions) is clearly present in Figures 2a, 2b, and 2c. Comparing Figure 2a with Figure 2b, it is clear that electrons have diffused inward toward the central wake (labeled as "Electrons diffuse ahead of ions"). In Figure 2c, the electron cloud is clearly indicated by the region in dark blue (more negative) located along the flanks of the wake. While there is a bulk electron flow inward ahead of the ions, there are also isolated pockets of electrons (in Figures 2b and 2c) that precede the primary electron flow. These are the fastest electrons originating from the ambient plasma at the wake flank. Because of the discrete nature of a PIC simulation, the tail of the electron velocity distribution (where the electron density is low) is not completely filled in, but instead appears as a few, discrete, fast particles, like those shown. If more particles were used, the region would appear as a continuum of electrons with no spatial gaps.

[13] Figure 2c indicates the presence of a region adjacent to the electron cloud where the density of ions exceeds that of the electrons (green region adjacent to cloud). The movement of electrons ahead of the main plasma will create a region where $n_i > n_e$ just behind the cloud, which is evident in this green region. These two adjacent regions of positive and negative excess charge form a standing double-layer structure trailing the obstacle. Evidence for this double

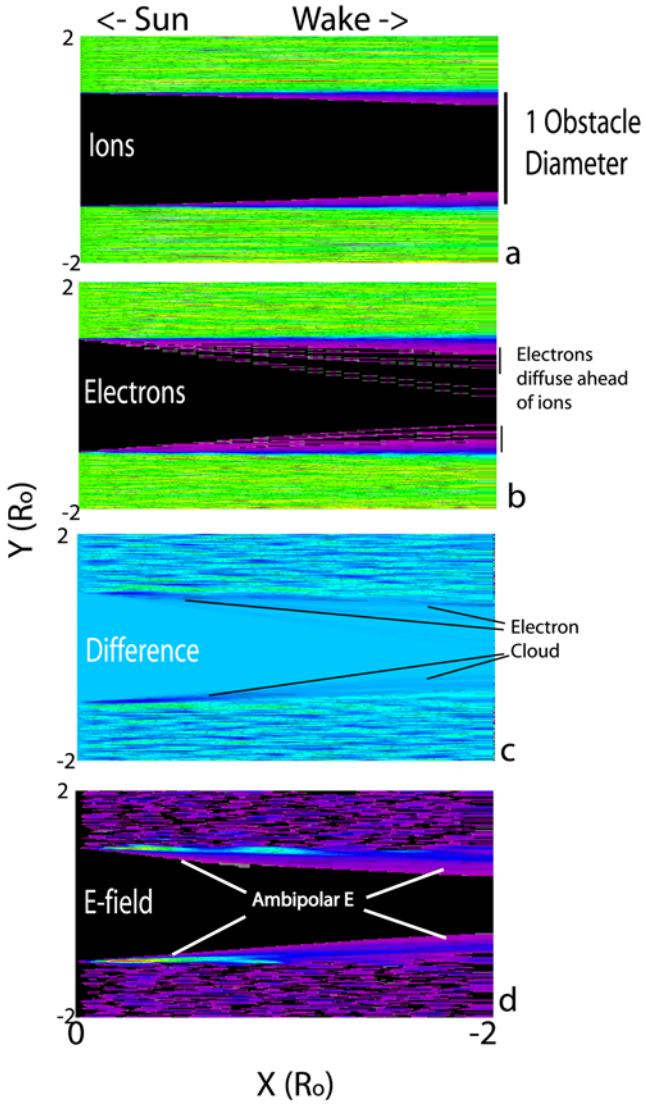

Figure 2. Simulation results showing a map of the (a) ion density, (b) electron density, (c) their differences, and (d) associated E-field downstream of the obstacle. Note that the E-field is strongest where the density differences are the greatest. In Figures 2a and 2b, green tones represent ambient plasma levels, while light blue, dark blue, and violet represent progressively decreasing levels to black (no particles). In Figure 2c, blue represents no difference, while green represents a slightly positive difference value and dark blue a slightly negative difference value. In Figure 2d, black represents no field, and purple, light blue, yellow and red represent increasing large E-field values (max at 20 sim units).

layer is the ambipolar electric field (Figure 2d) which maximizes at the boundary between excess-positive and excess-negative charge regions. This E-field also identifies the region where there is a loss of neutrality, with the fields naturally forming where the charge imbalance exists. The simulation shows a time-stationary situation, hence the E-field is a time-stationary structure, ever-present along the near-surface wake flank while flowing plasma is passing by the obstacle. Peak values of the E-field are near ~400 mV/m at X ~ −0.2 R_o.

[14] Figure 3 shows detailed profiles of n_e, n_i (overlaid) and E across the wake at downstream locations of 0.1, 0.2, and 1.8 R_o. Note that in Figures 3a and 3b, the profiles of density nearly perfectly overlap each other, except at the very edge of the wake, where electron densities (identified as "e-cloud" in the figure) exceed the ion densities. At these locations, the electrons extend further into the wake ahead of the ions. This electron-dominated plasma is the "electron cloud" discussed by *Crow et al.* [1975]. Also plotted is the E-field, which maximizes at the locations near the electron cloud.

[15] Based on the simulated electron distributions, the electron cloud is characterized by an ion-depleted, low density plasma (<10% of the ambient electron density) and appears to form as an inward directed beam. We recognize that the use of the term "cloud" to define a beam

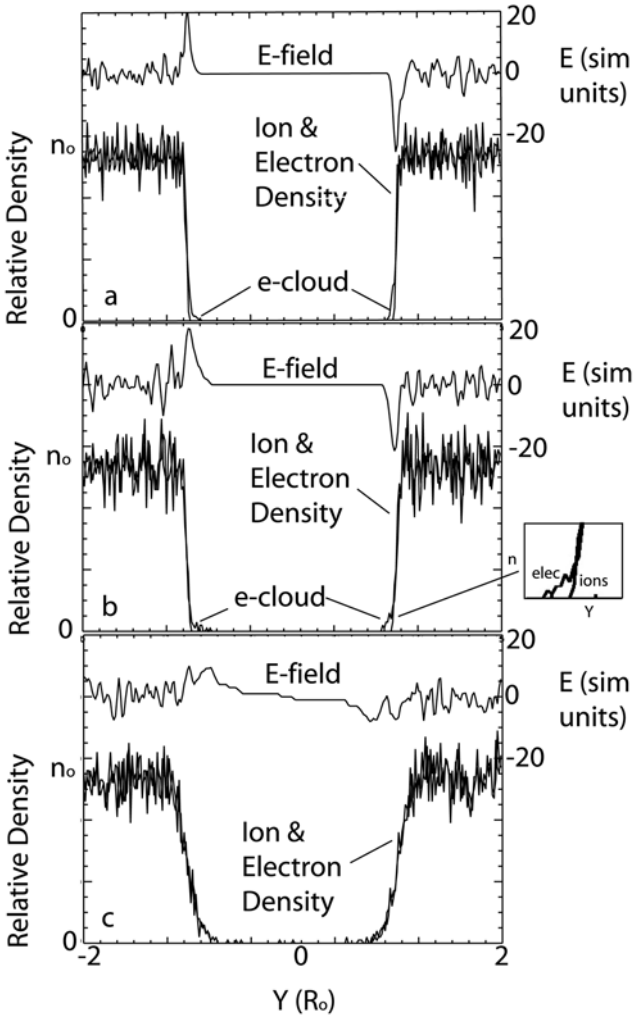

Figure 3. Slices across the wake at X = 0.1, 0.2 and 1.8 R_o. Electron and ion density profiles are overlaid and the presence of the electron cloud (e-cloud) along the wake flank is clear and distinct. The simulated E-field also peaks in the region near the electron cloud. Note that each unit of simulated E-field translates to ~20 mV/m (maximum field thus near ~400 mV/m).

may seem counter-intuitive. The electron ''cloud'' was originally identified by *Crow et al.* [1975] but the detailed electron distribution relative to the originating plasma was not compared. We now recognize the ''cloud'' as really in the form of an electron beam. The creation of the beam is straightforward to understand in terms of a time-of-flight effect: Given a thermal electron energy distribution at the edge of the wake flank, only those electrons at the distribution's tail have the necessary energy to propagate inward to the observation point consistent with the electron cloud. Hence, the cloud consists of the most energetic, tail electrons with the rest of the solar wind electron distribution subtracted out (since these do not have the energy to propagate to the observation point). This velocity filtration process effectively forms a beam with speeds near 1–2 times the electron thermal speed. This time-of-flight effect is clearly evident in the simulated distributions, with the electron beam velocity increasing with increasing distance from the wake flank. At the very edge of the electron cloud, the electron beam is in its most pure form, being a very low density, fast beam (with beam speeds near $\sim 2\ v_{te}$).

[16] The temperature of the electron cloud/beam is difficult to determine directly from the simulation, due simply to the low numbers of simulated cloud electrons. However, given the velocity filter effect described above, the temperature of the filtered beam can be inferred. The effective temperature of a plasma can be defined as $kT = -(d(\ln(f)/du)^{-1}$, where f is the electron energy distribution and u is energy. For an ambient plasma consisting of an isothermal Maxwellian distribution, the filtered electrons in the cloud are also isothermal beams since d(ln f)/du = constant. In contrast, kappa distributions like those found in the solar wind have d(ln f)/du decreasing with increasing energy making that filtered portion of the distribution effectively warmer than the original distribution. Hence, the electron cloud/beam effective temperature should rise as the structure moves inward toward the wake center.

4. Surface Potential

[17] The simulation was run with the initial condition that a void was present and the flanking plasma was then allowed to expand back into the void based on its own self-consistent ambipolar forces. For the lunar case, the expanding plasma immediately behind the terminator flows onto the lunar surface and as a consequence charges the surface to a potential that causes all incident currents to equal zero (current balance) at the local surface boundary [e.g., *Manka*, 1973]. We do not include the effect of a solid body in this simulation. However, the effect of the plasma on the lunar surface can be estimated using simulated ions and electrons at locations where the surface would exist. We then analytically calculate the surface charging using the simulated plasma as initial conditions.

[18] Specifically, within the cloud region, the surface potentials will become anomalously large and negative. The surface potential forms to keep current balance and varies as $e\varphi = -k\ T_e\ \ln(n_e v_e / n_i v_i)$ where n is the density, v is the beam speed, and e & i identify electron and ion components respectively [*Manka*, 1973]. As n_i decreases, φ becomes increasingly negative.

[19] The electron and ion densities near the surface at locations nightside of the terminator were determined from the simulation. The ratio of wake-to-ambient electron density is 0.71, 0.28, 0.19, and 0.13 at locations in the simulation corresponding to surface points of 5°, 10°, 15°, and 20° nightside from the terminator, respectively. For the self-similar fluid models like that by *Samir et al.* [1983], it is assumed that ion densities equal the electron densities. However, in the simulation of ambipolar expansion were quasi-neutrality is relaxed, we find wake-to-ambient ion density ratios of 0.47, 0.02, <0.02 (no simulated ions) and <0.02 (no simulated ions) at these same surface locations. Hence, electrons densities exceed ion densities by factors of $\sim$2 at 5° behind the terminator and factors of $\sim$15 at 10° behind the terminator.

[20] For self-similar models that keep the electron and ion densities equal [*Farrell et al.*, 2007], the surface potentials, $\varphi_{neutral}$, are −90 V, −110 V, −130 V, and −155 V at locations corresponding to surface points of 5°, 10°, 15°, and 20° from the terminator. However, if we now relax this constraint and use the simulated density ratios, we find the new surface potentials are increasingly negative, being −96 V, −160 V, <−180 V, and <−205 V at these same respective surface locations. Note that there are regions where n_i goes to zero making φ (in theory) negatively infinite. This limiting case does not really occur: current balance at the surface is then likely maintained by secondary electrons created from surface interaction with the primary electron cloud. We do not model the secondary electron processes herein, but suggest that surface potentials calculated at 15° with <−180 V and 20° with <−205 V may be far more negative than our bounding limits imply. Note that the surface potential analysis is for a nominal solar wind/solar environment and these potential values can become even more negative during a solar storm [*Halekas et al.*, 2007].

5. Conclusions

[21] Using an electrostatic particle-in-cell code, we examine the detailed processes associated with plasma expansion into a void. We focus on the activity occurring immediately following the points of initial plasma expansion, and our applications are ultimately directed toward the terminator/polar regions of the Moon. We find the following: (1) The development of an electron cloud that propagates ahead of the expanding plasma and, via time-of-flight processes, forms an inward directed (toward the central wake) electron beam, (2) the formation of a standing double layer and associated ambipolar electric field that spans from the electron cloud to the wake flank, and (3) surface potentials in the terminator region that becomes more negative in the presence of this electron cloud. NASA plans to build a lunar outpost in the polar Shackleton crater region, and surface locations near this base will be exposed to the wake-generated electron cloud and enhanced negative surface charging. Such large negative surface charging can accelerate dust grains to many 100's of meters per second [*Farrell et al.*, 2007], vertically loft grains to nearly 100 km [*Stubbs et al.*, 2006] and may give rise to the dusty sleet detected by Apollo 17's Lunar Ejecta and Meteorite (LEAM) experiment [*Berg et al.*, 1976]. An orbiting space-

craft with an E-field system should be capable of detecting the electron cloud regions with electron densities <0.5 electrons per cc and associated ambipolar E-fields ~0.4 V/m, thereby verifying the model results.

References

Benson, J. (1977), Direct measurement of the plasma screening length and surface potential near the lunar terminator, *J. Geophys. Res.*, *82*, 1917.

Berg, O. E., et al. (1976), Lunar soil movement registered by the Apollo 17 cosmic dust experiment, in *Interplanetary Dust and Zodiacal Light*, edited by H. Elsasser, et al., p. 233, Springer, Berlin.

Birch, P. C., and S. C. Chapman (2001a), Particle-in-cell simulations of the lunar wake with high phase space resolution, *Geophys. Res. Lett.*, *28*, 219.

Birch, P. C., and S. C. Chapman (2001b), Detailed structure and dynamics in particle-in cell simulations of the lunar wake, *Phys. Plasmas*, *8*, 4551.

Crow, J. E., P. L. Auer, and J. E. Allen (1975), The expansion of plasma into a vacuum, *J. Plasma Phys.*, *14*, 65.

Farrell, W. M., M. L. Kaiser, J. T. Steinberg, and S. D. Bale (1998), A simple simulation of a plasma void: Applications to Wind observations of the lunar wake, *J. Geophys. Res.*, *103*(A10), 23,653.

Farrell, W. M., T. J. Stubbs, R. R. Vondrak, G. T. Delory, and J. S. Halekas (2007), Complex electric fields near the lunar terminator: The near-surface wake and accelerated dust, *Geophys. Res. Lett.*, *34*, L14201, doi:10.1029/2007GL029312.

Halekas, J. S., S. D. Bale, D. L. Mitchell, and R. P. Lin (2005), Electrons and magnetic fields in the lunar plasma wake, *J. Geophys. Res.*, *110*, A07222, doi:10.1029/2004JA010991.

Halekas, J. S., G. T. Delory, D. A. Brain, R. P. Lin, M. O. Fillingim, C. O. Lee, R. A. Mewaldt, T. J. Stubbs, W. M. Farrell, and M. K. Hudson (2007), Extreme lunar surface charging during solar energetic particle events, *Geophys. Res. Lett.*, *34*, L02111, doi:10.1029/2006GL028517.

Manka, R. H. (1973), Plasma and potential at the lunar surface, in *Photon and Particle Interactions With Surfaces in Space*, edited by R. J. L. Grard, p. 347, Dordrecht, Netherlands.

Ogilvie, K. W., J. T. Steinberg, R. J. Fitzenreiter, C. J. Owen, A. J. Lazarus, W. M. Farrell, and R. B. Torbert (1996), Observations of the lunar plasma wake from the Wind spacecraft on December 27, 1994, *Geophys. Res. Lett.*, *23*, 1255.

Samir, U., K. H. Wright Jr., and N. H. Stone (1983), The expansion of a plasma into a vacuum: Basin phenomena and processes and applications to space plasma physics, *Rev. Geophys.*, *21*, 1631.

Singh, N., K. H. Wright Jr., N. H. Stone, U. Samir, and K. S. Hwang (1989), On the interpretation of measured ions streams in the wake of the shuttle orbiter in terms of plasma expansion processes, *J. Geophys. Res.*, *94*, 12,075.

Stubbs, T. J., R. R. Vondrak, and W. M. Farrell (2006), A dynamic fountain model for lunar dust, *Adv. Space Res.*, *37*, 59.

M. R. Collier, W. M. Farrell, T. J. Stubbs, and R. R. Vondrak, Solar System Exploration Division, NASA Goddard Space Flight Center, Greenbelt, MD 20771, USA. (william.farrell@gsfc.nasa.gov)

G. T. Delory, J. S. Halekas, and R. P. Lin, Space Science Laboratory, University of California, Berkeley, 7 Gauss Way, Berkeley, CA 94720–7450, USA.